On-Orbit Calibration of Photodiodes for Attitude Determination

John C. Springmann
Aerospace Engineering, University of Michigan
1320 Beal Ave, Ann Arbor, MI 48109; 734-647-7148
jspringm@umich.edu

Faculty Advisor: James W. Cutler
Aerospace Engineering, University of Michigan

ABSTRACT

This paper presents a method for on-orbit calibration of photodiodes for sun sensing in an attitude determination system. The calibration estimates the scale factors and alignment angles of the photodiodes, resulting in higher attitude determination accuracy than achieved with the pre-flight calibration parameters. The calibration is implemented with an extended Kalman filter to simultaneously estimate spacecraft attitude and the calibration parameters. This approach, as opposed to an attitude-independent method, enables the calibration of an arbitrary number of photodiodes mounted in any orientation on the spacecraft and facilitates the use of an attitude-dependent Earth albedo model. The method is demonstrated by application to flight data from the RAX-2 satellite and results in an average angular improvement of 10° in sun vector measurements with the photodiodes. Attitude determination accuracies of below 1° in each axis are demonstrated using the calibrated photodiodes in combination with a low-cost three-axis magnetometer and rate gyroscope.

I. INTRODUCTION

Sun sensors are the most widely used sensor type in attitude determination systems [1]. They are used to measure the vector from the spacecraft to the sun (herein referred to as the sun vector) in the spacecraft body-fixed frame, and their angular accuracies range from several degrees to less than an arc-second. Photodiodes, which generate current as a function of incoming light [2], are the most basic type of sun sensor. A stand-alone photodiode provides a measurement of the angle between the sun vector and the direction normal to the photosensitive plane, effectively measuring one component of the sun vector. For multi-axis sun sensing with photodiodes, two common schemes exist: (1) individual photodiodes can be mounted in different orientations – either within a single sensor package [3] or distributed over the spacecraft body [4] – for up to three-component sun sensing, or (2) multiple photodiodes and a mask can be combined within a single sensor package for two-axis sun sensing. The angular accuracy of the former scheme is on the order of degrees, and the angular accuracy of the latter depends on the complexity of the sensor [5, 6]. A photodiode-based sensor with accuracy on the order of degrees is typically referred to as a coarse sun sensor, whereas sensors with angular accuracies on the order of tenths of degrees or better are referred to as fine sun sensors. Fine sun senors commonly utilize more advanced components than photodiodes, such as CMOS sensors [7].

This work focuses on coarse sun sensors composed of individual photodiodes mounted at different angles. This photodiode scheme is extremely common on CubeSats and other small spacecraft [8–12] because of its simplicity and low cost[1]. One configuration that is typical of CubeSats is to mount the photodiodes orthogonal to each other by placing one on each surface of the spacecraft [8, 9, 12]. However, this configuration does not provide three-component sun sensing in all directions because the conical field of view of photodiodes is typically less than 180° [9]. A natural improvement to this is to use additional photodiodes mounted in various orientations over the spacecraft body to achieve three-component sun sensing in all directions. In addition to enabling three-component sun sensing, this configuration provides more information for the attitude determination system, resulting in a potential angular accuracy improvement. This photodiode scheme has been used on various spacecraft [3, 10, 13], and a design method to determine optimal photodiode orientations for sun sensing is given in Reference 4.

There are two parameters critical for accurate sun sensing with photodiodes: the scale factor and the ori-

[1] Osram SFH 2430 photodiodes, which flew on the RAX satellites [9], can be purchased for $1.84 per sensor (http://www.digikey.com/product-detail/en/SFH%202430-Z/475-2579-1-ND/1228076, accessed March 2013).

entation of each photodiode on the spacecraft. The scale factor is dependent on the characteristics of both the photodiode and surrounding circuitry, and it will be discussed further in Section III.B. Although the scale factor can be estimated from pre-flight calibration, photodiodes are known to degrade on-orbit due to radiation, and previous flight experience demonstrates that this has a significant effect on the scale factor [14]. Additionally, thorough pre-flight calibration requires a light source that is calibrated to match the characteristics of sunlight in orbit. On-orbit estimation of the scale factor provides the best estimate of the on-orbit sensor characteristics and lowers spacecraft development time and cost by mitigating rigorous pre-flight calibration requirements. Similarly, the pre-flight orientation of the photodiodes is known if sufficiently high tolerance procedures are used during spacecraft integration, but any high-tolerance procedures that add cost to the integration defeat the low-cost benefits of photodiodes, and the orientation may change during launch regardless of the initial tolerance. Therefore, the photodiode orientation is also estimated in flight.

In this work, we formulate and apply a method for on-orbit photodiode calibration to estimate the photodiode scale factor and orientation. The method is demonstrated by application to flight data from the RAX-2 satellite, and an average of 10° improvement in accuracy of the photodiode-based sun vector measurement is achieved. The remainder of this paper is organized as follows. Existing calibration techniques and the motivation for formulating the photodiode calibration as a recursive attitude-dependent method is discussed in Section II. The calibration technique is presented in Section III and applied to flight data in Section IV. A discussion of some of the assumptions and techniques used in the calibration is presented in Section V, and conclusions are given in Section VI.

II. EXISTING CALIBRATION TECHNIQUES

In general, sensor measurements are corrupted by errors such as scale factors, bias, and angular misalignments. Calibration is used to estimate and subsequently compensate for the sensor errors, and it is critical for accurate attitude estimation. Many calibration techniques have been presented in the literature; this section is not meant to include an exhaustive overview of existing calibration techniques, but rather to summarize the most relevant types of methods in the context of the new photodiode calibration presented in this paper.

The calibration process consists of modeling the sensor of interest and estimating the parameters of the model using sensor measurements from either ground-based testing or on-orbit operations. Calibration using only on-orbit data is referred to as *on-orbit* calibration, and it is advantageous over ground-based calibration because it accounts for any changes in sensor characteristics once they are in orbit, and it reduces satellite development time and cost by mitigating the pre-flight calibration requirements.

On-orbit calibration techniques can be categorized as either attitude-independent or attitude-dependent. Attitude-independent calibration does not require attitude knowledge and is accomplished by minimizing a scalar objective function that is dependent on the calibration parameters. For example, the angle between two vectors in the same frame does not depend on their frame of reference, so calibration can be carried out by minimizing the difference in angles between two measured vectors in the body-fixed frame and the two corresponding known reference vectors. This technique has been used to estimate sensor mis-alignments and other error parameters [15, 16]. Another common scalar objective function is the expected magnitude of the measured vector. For example, a common magnetometer calibration technique is to minimize the difference between the expected and measured magnitude of Earth's magnetic field as a function of the calibration parameters [17–19]. Both of these attitude-independent methods can be applied to various types of three-axis sensors. Attitude-dependent techniques are recursive methods that use attitude estimates for the sensor calibration, and thus simultaneously estimate attitude and sensor calibration parameters. Examples of this approach include References 20 and 21, which utilize an extended Kalman filter and an unscented filter, respectively, to estimate sensor mis-alignments, rate gyroscope scaling and bias, and attitude.

Regarding sun sensors specifically, on-orbit calibration of coarse sensors is not prevalent in the literature. Furthermore, the models of fine sun sensors are dependent on the sensor design, so existing calibration methods are typically applicable to only specific sensors [5, 6]. While both the attitude-independent and -dependent calibration approaches mentioned previously can be applied to on-orbit sun sensor calibration, direct application of these methods requires a sun sensor that provides a three-component sun vector measurement [22, 23]. Since photodiodes provide a measurement of a single sun vector component, a three-component measurement is not always available, making application of these methods non-trivial.

The on-orbit calibration method presented in this paper has been developed for stand-alone photodiodes in any orientation and does not require simultaneous illumination of multiple sensors, which would be required for a three-component vector measurement. An attitude-dependent approach is used because it enables the calibration of an arbitrary number of illuminated sensors and it also facilitates the use of an attitude-dependent Earth albedo model. Earth albedo is reflection of sunlight from

Earth's surface, and it can significantly degrade the accuracy of photodiode-based sun sensing. Both of these aspects are discussed in more detail with the calibration methodology in the next section.

III. FORMULATION OF THE ATTITUDE ESTIMATION AND CALIBRATION FILTER

On-orbit photodiode calibration is achieved by estimating the calibration parameters and spacecraft attitude simultaneously. This is a non-linear recursive state estimation problem where the states consist of the calibration parameters as well as spacecraft attitude and angular rates, and the state estimation utilizes sensor measurements and a model of the system. The extended Kalman filter (EKF) is a widely-used approach for this type of problem and has become a standard method for satellite attitude determination [24]. Our approach to the photodiode calibration is to combine the calibration with an existing EKF-based attitude estimation method, which is a similar formulation to that of other attitude-dependent on-orbit calibration techniques [20, 21]. We also developed an unscented filter (UF) for the calibration by combing the calibration problem with an UF-approach to attitude estimation [25], but we found that the UF did not provide significantly higher accuracy state estimates than the EKF, and therefore, we present the EKF-based approach in this paper[2]. We give an overview of EKFs in Section III.A and then discuss the integration of the photodiode calibration into an EKF in Section III.B.

A. *EKF Overview*

A complete derivation and explanation of an EKF is beyond the scope if this paper, so we provide an overview of EKFs here while assuming the reader is familiar with both Kalman filtering theory and spacecraft attitude estimation [24, 26–28]. The general form of the EKF given here provides the foundation for the photodiode calibration implementation.

The EKF is used to estimate the states of a system with the dynamic model

$$\dot{\mathbf{x}}(t) = \mathbf{f}\left(\mathbf{x}(t), \mathbf{u}(t), t\right) + G(t)\mathbf{w}(t) \tag{1}$$

given measurements

$$\tilde{\mathbf{y}}_k = \mathbf{h}(\mathbf{x}_k) + \mathbf{v}_k \ , \tag{2}$$

where $\mathbf{x}$ is the $n \times 1$ state vector, $\mathbf{u}(t)$ is the control input, $\mathbf{w} \sim N(\mathbf{0}, Q(t))$ is the process noise amplified by gain $G(t)$, $\tilde{\mathbf{y}}_k$ is the $m \times 1$ measurement vector available at time k, $\mathbf{v}_k \sim N(\mathbf{0}, R_k)$ is the measurement noise, and $\mathbf{f}()$ and $\mathbf{h}()$ are nonlinear functions. The state estimation procedure is the following. First, the state estimate $\hat{\mathbf{x}}$ and state covariance matrix P are initialized as in Eq. (3). When a measurement is available, it is used to update the state estimate and covariance using Eqs. (4)-(7), where the superscripts $^-$ and $^+$ denote the quantities before and after the update. The updated estimate and covariance are then propagated until the time of the next available measurement using Eqs. (8)-(10). This process is repeated with all measurements over the desired time period [26].

$$\hat{\mathbf{x}}(t_0) = \hat{\mathbf{x}}_0 \ , \ P_0 = E\left\{\tilde{\mathbf{x}}(t_0)\tilde{\mathbf{x}}^T(t_0)\right\} \tag{3}$$

$$K_k = P_k^- H_k^T\left(\hat{\mathbf{x}}_k^-\right)\left[H_k\left(\hat{\mathbf{x}}_k^-\right) P_k^- H_k^T\left(\hat{\mathbf{x}}_k^-\right) + R_k\right]^{-1} \tag{4}$$

$$H_k\left(\hat{\mathbf{x}}_k^-\right) \equiv \left.\frac{\partial \mathbf{h}}{\partial \mathbf{x}}\right|_{\hat{\mathbf{x}}_k^-} \tag{5}$$

$$\hat{\mathbf{x}}_k^+ = \hat{\mathbf{x}}_k^- + K_k\left[\tilde{\mathbf{y}}_k - \mathbf{h}\left(\hat{\mathbf{x}}_k^-\right)\right] \tag{6}$$

$$P_k^+ = \left[I - K_k H_k\left(\hat{\mathbf{x}}_k^-\right)\right] P_k^- \tag{7}$$

$$\dot{\hat{\mathbf{x}}}(t) = \mathbf{f}\left(\hat{\mathbf{x}}(t), \mathbf{u}(t), t\right) \tag{8}$$

$$\begin{aligned}\dot{P}(t) = F(\hat{\mathbf{x}}(t), t)P(t) + P(t)F^T\left(\hat{\mathbf{x}}(t), t\right) \\ + G(t)Q(t)G^T(t)\end{aligned} \tag{9}$$

$$F\left(\hat{\mathbf{x}}(t), t\right) \equiv \left.\frac{\partial \mathbf{f}}{\partial \mathbf{x}}\right|_{\hat{\mathbf{x}}(t)} \tag{10}$$

A specific implementation of the EKF that has become a default method for attitude estimation is the multiplicative extended Kalman filter (MEKF) [24, 27, 28]. It is termed *multiplicative* because the attitude update utilizes quaternion multiplication in addition to the additive state update of Eq. (6) to maintain attitude matrix orthogonality constraints. The MEKF is a six-state filter that estimates spacecraft attitude and rate gyroscope bias using a three-axis rate gyroscope and at least one attitude/vector sensor. Unlike the general form of an EKF which combines a dynamic model with sensor measurements, the MEKF does not utilize a dynamic model. Instead, the bias-corrected gyroscope measurements are used directly to propagate the attitude kinematics, which alleviates the difficulties of accurately modeling spacecraft dynamics [27]. We use the same methods as the MEKF for attitude estimation within the photodiode calibration filter.

B. *Photodiode Calibration*

With the general form of the EKF in-hand, the key aspects of the photodiode calibration are the photodiode measurement model, states, and state update equations, each of which are presented in this section.

[2]Unscented filters have the potential to provide higher accuracy state estimates than the EKF, and they are known be particularly advantageous over the EKF for non-linear state estimation with poor initial conditions. In our application of the photodiode calibration, both magnetic and sun vector measurements are available to initialize the attitude estimate, meaning that the initial condition is sufficiently accurate for EKF convergence. In both simulated testing and application to flight data, we found that the differences between the EKF and UF for calibration were insignificant.

1. Measurement Model

The measurement model for a photodiode illuminated by only the sun is given by Eq. (11), where $\tilde{I}$ is the measured current output; E_{AM0} is the irradiance of the sunlight[3]; I_0 is the maximum current output of the photodiode; E_{cal} is a scaling parameter that relates the current output to the incident irradiance and is dependent on the specific photodiode and surrounding circuitry; $\mathbf{n}$ is the 3×1 unit vector that defines the direction normal to the photosensitive plane, herein referred to as the photodiode normal direction; $\mathbf{s}$ is the 3×1 unit sun vector; and η is zero mean Gaussian measurement noise [8]. Even though both $\mathbf{n}$ and $\mathbf{s}$ are unit vectors, they are not denoted with the common unit vector notation of $\hat{\mathbf{n}}$ and $\hat{\mathbf{s}}$ because the hat symbol $\hat{\cdot}$ is reserved to denote estimated quantities.

$$\tilde{I} = \frac{E_{AM0} I_0}{E_{cal}} \mathbf{n}^T \mathbf{s} + \eta \tag{11}$$

The quantity $\mathbf{n}^T\mathbf{s}$ is equivalent to $\cos(\theta)$, where θ is the angle between the two vectors. $\cos(\theta)$ is commonly used instead of $\mathbf{n}^T\mathbf{s}$ in photodiode models, and photodiodes are sometimes referred to as cosine detectors [1]. Phototiodes generate current anytime $0 < \theta \leq 90°$, but the output deviates from the cosine model of Eq. (11) at high angles. The photodiode field of view (FOV) is the conical region over which the cosine model is valid. The exact FOV varies by sensor, but a half angle of 60°-70° is typical.

Photodiodes in low-Earth orbit are also subject to illumination from sunlight reflected by the Earth, which is called Earth albedo [29]. The irradiance of Earth albedo can be up to 30-40% of the solar irradiance, resulting in a potentially significant degradation of a sun vector measurement if it is not accounted for. Albedo is typically treated as noise in attitude estimation, and this approach can be successful particularly when other attitude sensors are available to complement the photodiodes. But we have found that this approach is not sufficient for photodiode calibration, so we include a model of albedo in the filter to remove its contribution from the measurements. The albedo model used was developed by Bhanderi using Earth reflectivity measurements from NASA's Total Ozone Mapping Spectrometer, and the model has been verified through comparison to flight data from the Ørstead satellite [8, 29, 30]. The photodiode measurement model with the inclusion of Earth albedo is

$$\tilde{I} = \frac{I_0}{E_{cal}} \left(E_{AM0} \mathbf{n}^T \mathbf{s} + E_a \right) + \eta \,, \tag{12}$$

where the albedo irradiance E_a is given by Eq. (13).

[3]The subscript AM0 denotes air mass zero, meaning zero atmospheres. E_{AM0} is the solar irradiance at 1 AU with no loss due to Earth's atmosphere. The value is $E_{AM0} = 1367$ W/m^2 [8].

Earth albedo is a function of the relative positions of the Sun, Earth, and satellite, and the Earth reflectivity varies with longitude, latitude, and atmospheric conditions such as cloud coverage. To account for the varying reflectivity, Earth's surface is partitioned into cells and the reflectivity of each cell is the average of measurements over a one year time period. The latitude and longitude of the center of each cell is denoted by $(\phi_g, \theta_g) \in \mathcal{D}$, where $\mathcal{D}$ is the set of all cell locations. The incident Earth albedo irradiance on a photodiode with normal direction $\mathbf{n}$ is

$$E_a = \sum_{\mathcal{V}_{sun} \cap \mathcal{V}_{sat}} E_c \left(\phi_g, \theta_g \right) \mathbf{n}^T \mathbf{r}_g \,, \tag{13}$$

where $\mathcal{V}_{sun} \subset \mathcal{D}$ and $\mathcal{V}_{sat} \subset \mathcal{D}$ are the cells in the field of view of the Sun and satellite, respectively; E_c is the irradiance reflected by the g-th cell in the direction of $\mathbf{r}_g$, which is a function of the reflectivity of the cell, direction of incoming solar irradiance, and direction to the satellite; and $\mathbf{r}_g$ is the vector from the satellite to the center of the cell. The details of the model development and calculation of E_c can be found in the existing literature [8, 30].

The critical aspect of a photodiode measurement for attitude determination is the sun vector component along the photodiode normal direction, $\mathbf{n}^T\mathbf{s}$. This quantity can also be written as a function of spacecraft attitude and the sun vector in the inertial reference frame, which is a known function of time and satellite position. This is given by Eq. (14), where $|_B$ indicates that the preceding quantity is resolved in the satellite body-fixed frame, $|_R$ indicates that the quantity is resolved in the inertial reference frame, and A is the 3×3 proper orthogonal attitude matrix defining the orientation of the body-fixed frame relative to the reference frame.

$$\left(\mathbf{n}^T \mathbf{s} \right) \big|_B = \mathbf{n}^T \big|_B \, A \, \mathbf{s} \big|_R \tag{14}$$

The measurement model that relates the photodiode measurement to spacecraft attitude (analogous to Eq. (2) of the EKF general form) is obtained by substituting Eq. (14) into Eq. (12). The result is given by Eq. (15), where the i subscripts indicate that the terms are specific to the i-th photodiode and the substitution $C_i = \frac{E_{AM0} I_{0,i}}{E_{cal,i}}$ has been used. C_i is the sensor scale factor that will be estimated with on-orbit calibration. It is a dimensional scale factor that is equivalent to the maximum current output caused by irradiance of only direct sunlight.

$$\tilde{I}_i = C_i \mathbf{n}_i^T A \, \mathbf{s} \big|_R + C_i \frac{E_{a,i}}{E_{AM0}} + \eta \,. \tag{15}$$

As discussed in Section I, C_i and $\mathbf{n}_i$ in Eq. (15) are critical for accurate attitude determination and will be estimated along with A from the on-orbit measurements within the EKF.

2. State Dynamics

The conventional MEKF estimates six states: the 3×1 attitude error vector $\mathbf{a}$, which in combination with quaternions being propagated within the filter, quantifies spacecraft attitude [27, 28], and the 3×1 rate gyroscope bias $\boldsymbol{\beta}$. For photodiode calibration, we use the same states as the MEKF and include the calibration parameters as additional states. The photodiode normal directions $\mathbf{n}_i$ are parametrized by their corresponding azimuth and elevation, α_i and ϵ_i, respectively. This is given by Eq. (16).

$$\mathbf{n}_i = \begin{bmatrix} \cos(\epsilon_i)\cos(\alpha_i) & \cos(\epsilon_i)\sin(\alpha_i) & \sin(\epsilon_i) \end{bmatrix}^T \tag{16}$$

Azimuth and elevation are used rather than the three-component normal vector because three components of a unit vector are not linearly independent. The full state vector is then

$$\mathbf{x}_{(6+3m_p)\times 1} = \begin{bmatrix} \mathbf{a}^T & \boldsymbol{\beta}^T & \mathbf{C}^T & \boldsymbol{\alpha}^T & \boldsymbol{\epsilon}^T \end{bmatrix}^T , \tag{17}$$

where m_p is the total number of photodiodes included in the attitude determination system and

$$\mathbf{C} = \begin{bmatrix} C_1 \\ \vdots \\ C_{m_p} \end{bmatrix} , \ \boldsymbol{\alpha} = \begin{bmatrix} \alpha_1 \\ \vdots \\ \alpha_{m_p} \end{bmatrix} , \ \boldsymbol{\epsilon} = \begin{bmatrix} \epsilon_1 \\ \vdots \\ \epsilon_{m_p} \end{bmatrix} . \tag{18}$$

The attitude and gyro bias states are propagated in the same manner as the MEKF [27, 28]. The azimuth and elevation of each sensor is expected to remain constant over time (assuming they are not mounted on actuated surfaces). The scale factor is expected to decrease over time due to radiation, but since the degradation is much slower than the frequency of measurements, process noise is sufficient to capture the degradation. The dynamic models of the calibration states are therefore given by Eq. (19), where $\mathbf{w}_C$, $\mathbf{w}_\alpha$, and $\mathbf{w}_\epsilon$ are each mean zero Gaussian random vectors.

$$\dot{\mathbf{C}}(t) = \mathbf{w}_C \ , \ \ \dot{\boldsymbol{\alpha}}(t) = \mathbf{w}_\alpha \ , \ \ \dot{\boldsymbol{\epsilon}}(t) = \mathbf{w}_\epsilon \tag{19}$$

3. State Update and Propagation

As seen in Eqs. (5) and (10), partial derivatives of the measurement model and state dynamics are used in the EKF. The partial derivatives that make up the photodiode portion of the sensitivity matrix H are

$$\frac{\partial \tilde{I}_i}{\partial \mathbf{a}} = C_i \mathbf{n}_i^T \left[(A\ \mathbf{s}|_R) \times \right] , \tag{20}$$

$$\frac{\partial \tilde{I}_i}{\partial \boldsymbol{\beta}} = \mathbf{0}_{1\times 3} , \tag{21}$$

$$\frac{\partial \tilde{I}_i}{\partial C_i} = \mathbf{n}_i^T A\ \mathbf{s}|_R \ , \tag{22}$$

$$\frac{\partial \tilde{I}_i}{\partial \alpha_i} = C_i \begin{bmatrix} -\cos(\epsilon_i)\sin(\alpha_i) \\ \cos(\epsilon_i)\cos(\alpha_i) \\ 0 \end{bmatrix}^T A\ \mathbf{s}|_R \ , \tag{23}$$

$$\frac{\partial \tilde{I}_i}{\partial \epsilon_i} = C_i \begin{bmatrix} -\sin(\epsilon_i)\cos(\alpha_i) \\ \sin(\epsilon_i)\sin(\alpha_i) \\ \cos(\epsilon_i) \end{bmatrix}^T A\ \mathbf{s}|_R \ . \tag{24}$$

Eq. (20) is derived using the same methods as other vector measurements in the MEKF [28], and the $\times$ denotes the cross-product skew-symmetric matrix [26]. These partial derivatives ignore the albedo contribution in Eq. (15), which is a reasonable approximation since the direct Sun irradiance typically, though not always, dominates the measurements. Simulated testing has confirmed sufficient filter performance under this assumption.

The partial derivatives of the calibration parameter states for Eq. (10) are zero vectors. The partial derivatives of the attitude and gyro bias states are the same as in the MEKF and are derived in the existing literature [27, 28].

To implement the photodiode calibration, Eqs. (15)-(24) are integrated into the EKF with the general form of Eqs. (1)-(10). Other vector/attitude sensor measurements can also be used in the filter by appending them to the rows of the measurement vector $\tilde{\mathbf{y}}$ and sensitivity matrix H. In our simulated testing and application to on-orbit data, a three-axis magnetometer and multiple photodiodes were used in addition to the three-axis rate gyroscope for photodiode calibration and attitude estimation.

IV. FLIGHT DATA RESULTS

The calibration filter has been tested through simulation, and its utility has been demonstrated by application to flight data. For compactness, the simulation results are not presented here, but rather, we focus on the flight data results. The flight data is from RAX-2, which is discussed in Section IV.A. Results of the application to flight data are discussed in Section IV.B, and its impact on sun vector angular accuracy and the resulting attitude determination accuracy is presented in Section IV.C.

A. RAX-2 Data

The calibration filter is applied to data from the second Radio Aurora Explorer satellite, RAX-2 [13, 31]. RAX-2 is an operational 3U CubeSat developed to study space weather irregularities in Earth's ionosphere. It launched October 28, 2011 into an 102° inclination 400 $\times$ 820 km orbit. The attitude determination sensors are commercial off-the-shelf components and include an Analog

Devices ADIS16405 inertial measurement unit (which includes a three-axis gyroscope), a PNI MicroMag3 three-axis magnetometer, and 17 Osram SFH2430 photodiodes with solar cell coverglass attached to reduce the radiation-induced degradation. The design and implementation of the attitude determination subsystem on RAX-1 is discussed in Reference 9, and the RAX-2 subsystem is identical except it includes additional photodiodes with coverglass. RAX-1 utilized photodiodes mounted parallel to each of its six orthogonal faces. The additional photodiodes on RAX-2 are mounted at various angles to enable three-component sun sensing for nearly every direction in the body frame.

A photo of RAX-2 is shown in Figure 1. Six photodiodes are visible in the picture and are circled, and the body-fixed coordinate frame is shown. The angled photodiodes are mounted on Delrin wedges, soldered to the solar panels, and staked to the spacecraft. There are three photodiodes each on the x and y faces that are mounted in different orientations, and there are three on the $+z$ surface and two on the $-z$ surface that are mounted parallel to the surfaces. Redundant sensors were placed on the z surfaces to avoid shadows from antennas. The intended azimuth and elevation angles of the photodiode normal directions is given in Table 1. These angles were chosen because they provide three-component sensing over nearly the entire body frame while adhering to the CubeSat specifications that limit the height of objects mounted on the satellite surfaces. No high tolerance practices were used in mounting the photodiodes; the wedges were laser cut and mounted to the spacecraft by hand.

Data used in this section was downloaded from the spacecraft for satellite health assessment and sensor calibration, and the calibration was performed during ground-based analysis of the flight data. A discussion of real-time calibration and calibration via post-processing the data is included in Section V.

B. Application

Sensor calibration provides the most accurate results when using measurements throughout the full sensor field of view (for example, see the procedures of Ref. 18 or the observability discussion in Ref. 19). RAX-2 utilizes a passive magnetic control system that aligns the spacecraft to the geomagnetic field and dampens rotational kinetic energy within the first few weeks after deployment from the launch vehicle. Therefore, we use sensor data from early in the mission when the spacecraft is still tumbling for the calibration as this data includes measurements of the sun vector in nearly all directions of the body-fixed frame[4]. Two data sets of 1 Hz sample period and 120 minute duration were recorded during this time, and the subset of each data set when the spacecraft was in the sun (seen in Figure 2) is used for the calibration. The data sets begin Nov. 4, 2011 18:29:45 UT and Nov 12, 2011 18:33:00 UT, and are herein referred to data set one and two, respectively. The photodiode raw data from each data set is shown in Figure 2, and the corresponding measured sun vector directions are shown in Figure 3. These directions were estimated using the initial calibration parameters and the method of Ref. 4 to convert the photodiode measurements to sun vectors.

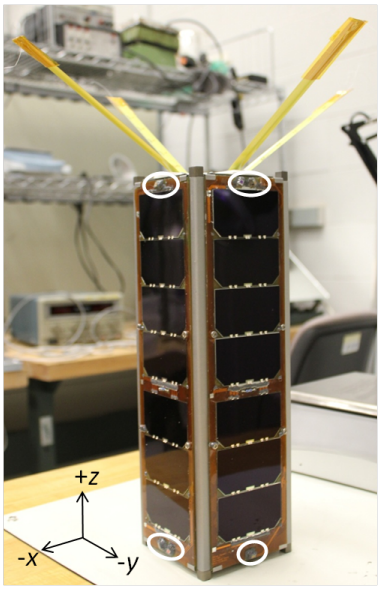

Figure 1. The RAX-2 satellite with the photodiodes circled.

Initial state estimates are required for the EKF. The initial estimate of the scale factor is taken to be the maximum measured output of each photodiode over the data set. Recall that this dimensional scale factor is equivalent to the maximum current output caused by direct sunlight (see Eq. (15)), so the maximum measured output while the spacecraft is tumbling provides a reasonable initial estimate. The initial estimate of azimuth and elevation are the intended mounting angles of Table 1. The initial attitude estimate is calculated from the measured magnetic and sun vectors using the q-method [24]. The magnetometers were first calibrated using an on-orbit, attitude-independent method [19], and the sun vector measurement for the initial attitude calculation utilizes the initial calibration parameters. The initial rate gyroscope bias is assumed to be zero. The magnetic and sun reference vectors were exported from AGI's Simulation Toolkit (STK) using two-line elements and the SGP4 propagator to estimate spacecraft position.

Filter tuning is the process of adjusting the covariance matrices Q and R (see Eqs. (1)-(2)) such that the

[4]For actively controlled spacecraft, maneuvers can be performed specifically for sensor and actuator calibration.

Table 1. The intended azimuth and elevation angles of the photodiode normal directions on RAX-2.

Photodiode #	1	2	3	4	5	6	7	8	9	10	11	12	13-15	16-17
α (deg)	17	0	-17	-162	180	162	72	107	90	-107	-72	-90	0	0
ϵ (deg)	-10	20	-10	-10	20	-10	10	10	-20	10	10	-20	90	-90

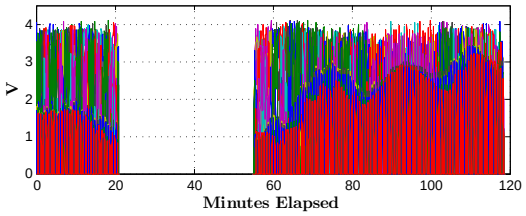

a) Data set one.

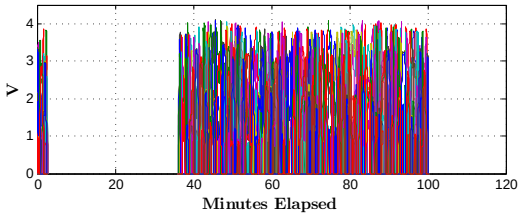

b) Data set two.

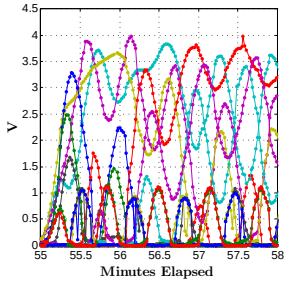

c) Zoomed-in portion of data set one.

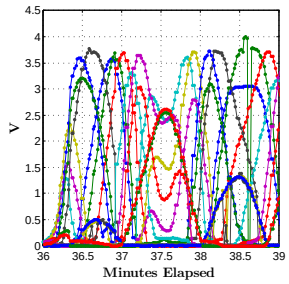

d) Zoomed-in portion of data set two.

Figure 2. Raw photodiode measurements (voltage) from data sets one and two. The times of the data used for calibration are 56-118 minutes for data set one1, and 37-100 minutes for data set two.

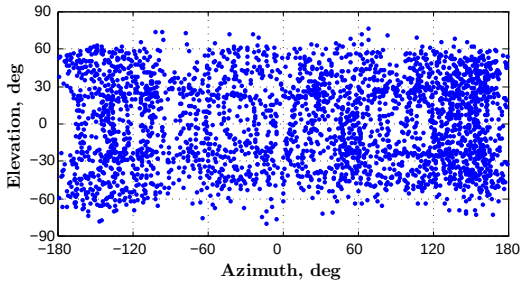

a) Data set one.

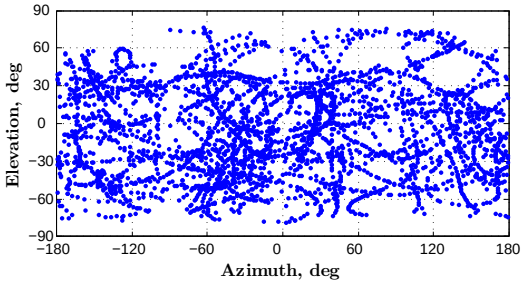

b) Data set two.

Figure 3. Measured sun vector directions in the body-fixed frame from each data set.

filter provides accurate state estimates. The criteria for an accurate and near-optimal EKF is that the state covariance must accurately quantify the state estimation error. During filter development through simulated testing, the true states are known (simulated) so the state covariance P can be compared directly to the true estimation error. Given the assumption of zero-mean Gaussian measurement and process noise in the filter, the state estimation error should also have a zero-mean Gaussian distribution with covariance given by P. This means that 99.7% of the state estimates should have error within the 3-σ (3 standard deviations) bound predicted by the covariance matrix [26]. During testing with simulated data similar to the flight data[5], the process covariance matrix Q was tuned until 99.7% of the state estimate errors were within the 3-σ bounds. This provided the initial Q used with the flight data. The initial measurement covariance matrix R is composed of the individual sensor uncertainties. The standard deviation of the PNI magnetometer measurements after on-orbit calibration [19] is approximately 320 nT, and from pre-flight testing, the approximate standard deviation of the individual photodiode measurements is 0.015 V. Volts are used rather than amps because even though the measurement model for photodiodes was given in terms of current, the voltage across a resistor is measured in their implementation, which is directly proportional to the current. To account for uncertainty in the Earth albedo model, an additional uncertainty corresponding to 50 W/m^2 is added to the photodiode measurement uncertainty. Using the initial estimate of the scale factors, 50 W/m^2 irradiance uncertainty corresponds to a photodi-

[5]During filter testing, the sensor sampling frequency, measurement noise, and satellite dynamics are simulated such that they are representative of the flight data.

ode output of 0.13 V, an order of magnitude greater than the individual photodiode uncertainty.

Since the true estimation error is unknown when using flight data, tuning is based on the measurement residuals. The photodiode measurement residuals are the difference between the measured vector components and the expected components given the estimated attitude. The measurement residuals of photodiode i are given by Eq. (25), which is derived from the measurement model of Eq. (15) and uses the state estimates since the true states are unknown. The magnetometer residuals are also used in filter tuning.

$$\varepsilon_{photodiode_i} = \tilde{I}_i - \hat{C}_i \hat{\mathbf{n}}_i^T \hat{A}\, \mathbf{s}|_R - \hat{C}_i \frac{E_{a,i}}{E_{AM0}} \qquad (25)$$

The measurement residuals are caused by both measurement uncertainty and uncertainty in the attitude estimate. In filter tuning, we adjust the process and measurement covariance such that the residuals are zero mean and within the total 3-σ bounds of the combined attitude estimate and measurement uncertainty. A sample of the measurement residuals of the tuned filter is shown in Figure 4.

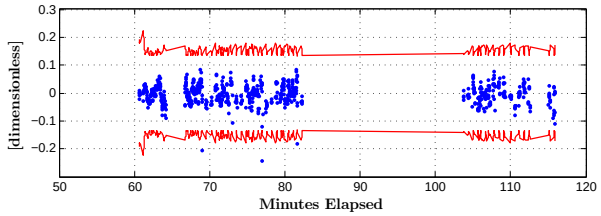

Figure 4. Measurement residuals (dots) and ±3-σ bounds (lines) from one of the photodiodes in data set one.

Plots of the state estimates over time from the tuned filter applied to data set one are shown in Figures 5-7. These show the state estimates for the first three photodiodes, and the behavior is representative of the estimates for all 17 photodiodes. In each plot, the estimate is shown only when a measurement is available for the state update (the estimate is constant at other times given Eq. (19)) and the predicted 3-σ bounds are shown over the duration of the data set. We see that the estimates converge to a consistent value within the first ten minutes of measurements. This, as well as the residuals criteria discussed previously, indicate that the filter is providing accurate state estimates.

We use two metrics as an additional verification of the accuracy of the state estimates. First, comparing the estimates of the azimuth and elevation from each data set, which we expect to be constant over time, the estimated 3-σ bounds overlap, which demonstrates consistency in the estimates. Additionally, the effectiveness of the calibration can be seen in comparing the measured sun vector

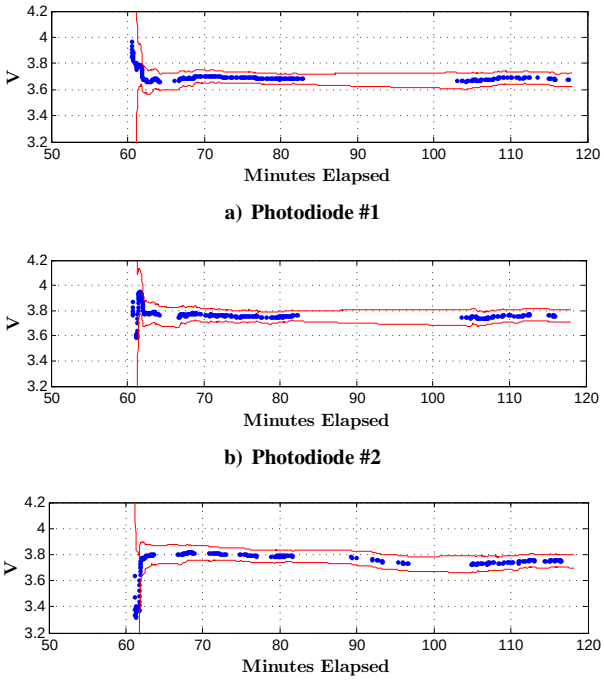

a) Photodiode #1

b) Photodiode #2

c) Photodiode #3

Figure 5. Scale factor estimates (points) and ±3-σ bounds (lines) for photodiodes 1-3 from data set one.

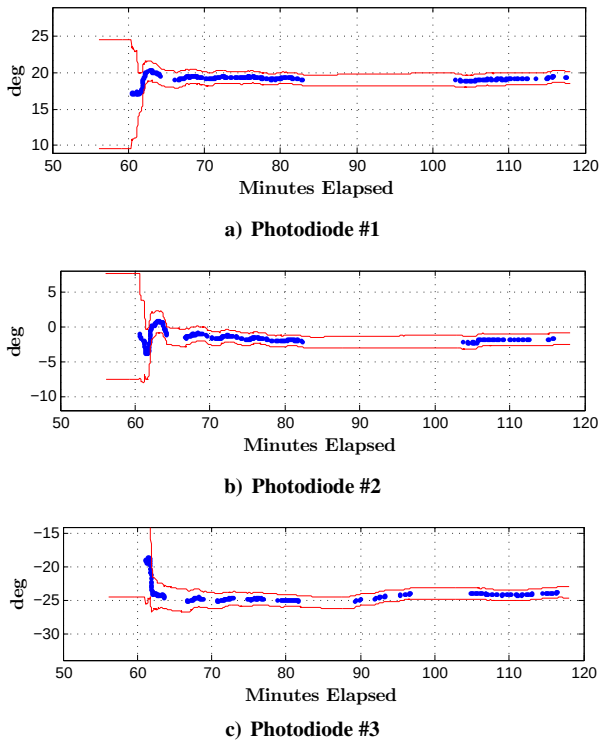

a) Photodiode #1

b) Photodiode #2

c) Photodiode #3

Figure 6. Azimuth estimates (points) and ±3-σ bounds (lines) for photodiodes 1-3 from data set one.

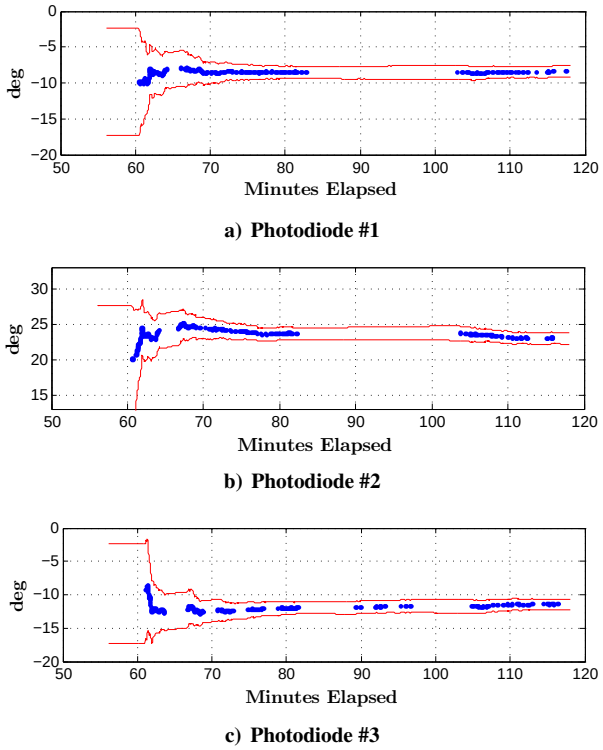

Figure 7. Elevation estimates (points) and ± 3-σ bounds (lines) for photodiodes 1-3 from data set one.

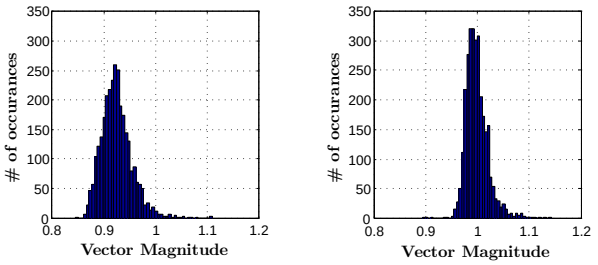

Figure 8. Histograms of the magnitude of the measured sun vector from data set one using the initial (left) and calibrated (right) sensor parameters.

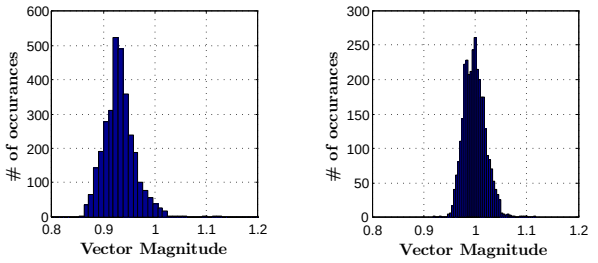

Figure 9. Histograms of the magnitude of the measured sun vector from data set one using the initial (left) and calibrated (right) sensor parameters.

magnitude using the initial and final calibration parameters, which is an attitude-independent verification metric. The magnitude of the measured sun vector should be one. Histograms of this vector magnitude[6], which was calculated with the albedo-corrected photodiode measurements and both the initial and calibrated photodiode parameters, are shown in Figures 8-9. In the first data set, the mean vector magnitude improves from 0.925 to 0.993, and the standard deviation decreases from 0.029 to 0.022 when using the on-orbit-estimated parameters rather than initial parameters. In the second data set, the mean improves from 0.932 to 0.999 and the standard deviation decreases from 0.032 to 0.021.

The importance of including Earth albedo in the calibration is evident by comparing the magnitude of the measured sun vector calculated with the raw photodiode measurements to the magnitude calculated with albedo-compensated measurements. This is shown in Figure 10 for both data sets. There are clear deterministic trends in the magnitude calculated from the uncompensated measurements that have been removed by subtracting the modeled albedo contribution from the measurements.

[6]The vector magnitude does not have a Gaussian distribution. The sum of the squares of components with Gaussian distributions has a chi-square distribution.

Since the albedo contribution is attitude-dependent, this demonstrates the need for simultaneous attitude estimation and calibration as opposed to an attitude-independent calibration. These trends were also seen in an initial attitude-independent attempt at calibrating the RAX-1 photodiodes [14], which required three simultaneously-illuminated sensors and did not account for Earth albedo. The new recursive method presented in this paper overcomes both the adverse affect of albedo and the need for multiple illuminated sensors in the calibration.

C. *Impact on Sun Vector Angular Accuracy and Attitude Determination*

The difference between the initial calibration parameters – which were the intended mounting angles and the maximum measured output of each photodiode while the spacecraft was tumbling – and the estimates from on-orbit calibration is significant. The improvement in elevation and azimuth estimates ranged from 0° - 9°, and the improvement in scale factor ranged from 0.17 - 0.46 V, which is equivalent to 4.4% - 12.7% of the calibrated scale factor. Histograms of angular differences between the measured sun vector using the initial and calibrated parameters for both data sets are shown in Figure 11. The mean improvement in sun vector angular accuracy is 9.1° and 10.2° from the two data sets, which is quite signifi-

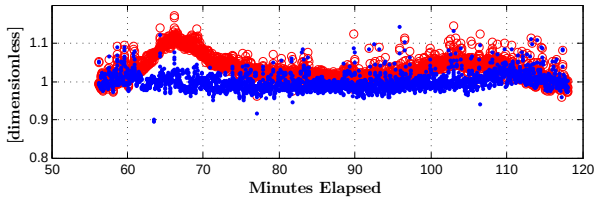

a) Data set one

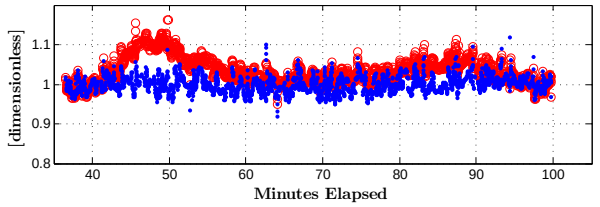

b) Data set two

Figure 10. Magnitude of the measured sun vector over time for the two data sets using both the uncompensated photodiode measurements (red circles) and the albedo-compensated measurements (blue dots). These magnitudes were calculated with the estimated calibration parameters. The albedo-compensated series of data is the same data as the calibrated histograms of Figures 8-9.

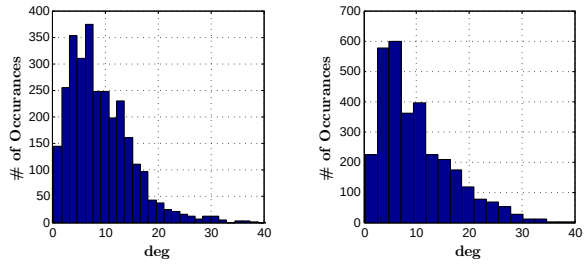

a) Data set one b) Data set two

Figure 11. Histograms of the angular difference between the measured sun vector using the initial and calibrated photodiode parameters. The mean from data set one is 9.1° and the mean from data set two is 10.2°.

cant given that the angular accuracy of photodiodes is on the order of degrees. The poor alignment of the photodiodes is not surprising given the manual process used to integrate them to the spacecraft. In application to other spacecraft, the degree of improvement resulting from the on-orbit calibration will be dependent on the quality of the pre-flight calibration parameters.

The 1-σ attitude estimation accuracy during the simultaneous attitude estimation and photodiode calibration is shown for both data sets in Figure 12. The three components are the uncertainty in rotation about the x, y, and z axes of the body-fixed frame. We see that the accuracy of the three components is better than 1° 1-σ for most of the duration that the spacecraft is in the sun. The periods of higher uncertainty between 90-100 minutes in data set one and 73-83 minutes in data set two are caused by the relative alignment of the sun vector and magnetic vectors in the body frame. During these time periods, the vectors are nearly parallel, significantly reducing the amount of information available for attitude determination.

The attitude accuracy is slightly better for data set two compared to data set one. This is because the spacecraft angular velocity is slower during data set two, but the rate gyroscope sampling frequency is the same for both data sets. Since the MEKF uses the gyro measurements directly in the attitude propagation, an inherent assumption is that the angular rate is constant between measurements. This is not the case if the sampling frequency is not high enough relative to the angular acceleration, which is the case for data sets one and two. This is compensated for in the filter by increasing the process covariance matrix to rely more heavily on the vector measurements than the gyro. Higher accuracy attitude estimation is achieved when the gyro measurements sufficiently capture the dynamics. This is demonstrated by Figure 13, which shows the attitude accuracy during a data set from later in the mission (Dec 9, 2011) after the passive magnetic control system had dampened the rotational kinetic energy and aligned the spacecraft z-axis with Earth's magnetic field. In filtering this data set, the full photodiode calibration filter was not used since the photodiode normal directions were estimated with the earlier data sets and are not expected to change over time. The scale factors were left as states in case of any on-orbit degradation of the photodiode output; these states were initialized to their on-orbit estimates from the earlier data sets. We see that the 1-σ attitude accuracy in the x- and y-axes is better than 0.5° when the spacecraft is in the sun. The z-axis (spin axis) has the least accuracy because the spacecraft is spinning about the magnetic vector, which minimizes the amount of non-redundant information that the gyroscope and magnetometer provide. The decrease in accuracy of all three components at 72 minutes is when the spacecraft enters eclipse and the photodiode measurements are no longer available.

V. DISCUSSION

We have utilized a three-axis rate gyroscope and three-axis magnetometer in addition to the photodiodes for the photodiode calibration. Since the calibration is a recursive method, either a rate gyroscope or a dynamic model is required for fusion with the vector measurements. Use of a rate gyroscope instead of a dynamic model has become a common approach for attitude estimation [27], but use of a dynamic model with no rate gyroscope has also been demonstrated [32, 33] and can be utilized for photodiode calibration with the formulation presented in Section III.B. The calibration can also be accomplished

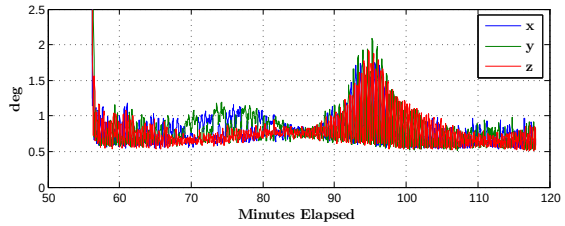

a) Data set one

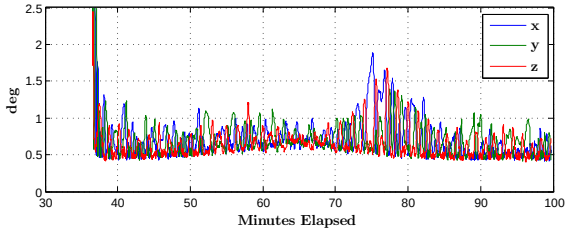

b) Data set two

Figure 12. Attitude accuracy (1-σ) achieved in applying the attitude estimation/calibration filter to data sets one and two.

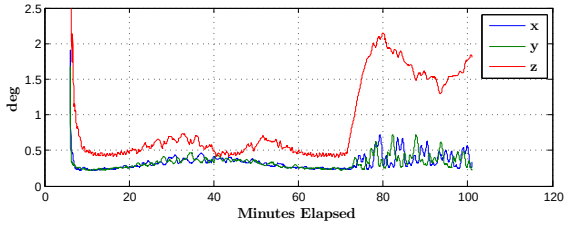

Figure 13. Attitude accuracy of a third data set, which was collected December 9, 2011 16:00:00 UTC.

without a magnetometer or other vector sensor, but the state estimation accuracy will be worse than with the additional attitude sensor since the sun sensors alone provide only two axis information (spin about the sun vector is the third axis). We included the magnetometer since it is available and results in significantly better accuracy compared to that using only the photodiodes. We have done initial testing of the calibration filter with only the gyroscope and photodiode measurements and have demonstrated convergence, but a thorough study on the accuracy when using photodiodes as the only vector measurement is left for future work.

In application of this calibration method to RAX-2, the flight data was downloaded from the spacecraft and processed on the ground. Real-time attitude estimation is not required on RAX-2, and downloading batches of data periodically throughout the mission is part of normal RAX-2 operations. Nonetheless, extended Kalman filters are well-suited for real-time implementation. Murrell's version of the EKF can be used to reduce the size of matrices required for inversion to 3×3 and discrete attitude propagation can be used to reduce the computational requirements [26]. The only aspect of the calibration method that is not well suited for on-line implementation in its current form is the Earth albedo model. For on-line implementation, the albedo model could be simplified [34] or pre-calculated and tabulated on-board. Investigation into these options is left for future work. Off-line calibration can be advantageous since it allows for a thorough inspection of the measurement residuals and tuning parameters, and real-time sensor correction can be accomplished even with off-line calibration by uploading the calibration parameters to the spacecraft.

In addition to attitude determination, the photodiode calibration can be used to track the orientation of actuated surfaces on a spacecraft. For example, if a photodiodes are placed on actuated solar panels, then the filter presented in this paper can be used to estimate the orientation of the actuated panels relative to the body-mounted attitude sensors.

VI. CONCLUSION

We have developed a method for on-orbit photodiode calibration to estimate the orientations and scale factors of photodiodes in an attitude determination system. The calibration utilizes an extended Kalman filter to simultaneously estimate spacecraft attitude and the calibration parameters, and it can be applied to any number of photodiodes in an arbitrary configuration on the spacecraft. In application to RAX-2, which utilizes photodiodes, magnetometers, and a three-axis rate gyroscope for attitude determination, the calibration improved the accuracy of the measured sun vector by an average of 10°. This calibration enables the most accurate performance of the attitude determination system with the given hardware. With the combination of calibrated photodiodes as well as a low-cost magnetometer and gyroscope, attitude accuracies of better than 1° 1-σ have been demonstrated.

ACKNOWLEDGEMENTS

This research is supported by the Department of Defense through a National Defense Science and Engineering Graduate (NDSEG) fellowship. RAX-2 was funded by the National Science Foundation. Thanks to Alex Sloboda and Alex Fox for providing feedback on this manuscript.

References

[1] Lerner, G. M., *Spacecraft Attitude Determination and Control*, chap. 6.1: Sun Sensors, Kluwer Academic Publishers, 1978, pp. 155–166.

[2] Dado, S. and Fischer, J., *Modern Sensors Handbook*, chap. 2.2.2: Light Detectors, ISTE Ltd, 2007, pp. 54–62.

[3] Tambo, T., Shibata, M., Mizuno, Y., and Yamauchi, T., "Search Method of Sun Using Fixed Five Photodiode Sensor," *IEEJ Transactions on Sensors and Micromachines*, Vol. 129, No. 2, 2009, pp. 53–59.

[4] Springmann, J. C. and Cutler, J. W., "Optimization of Directional Sensor Orientation with Application to Photodiodes for Spacecraft Attitude Determination," *Proceedings of the AAS/AIAA Spaceflight Mechanics Meeting*, Kauai, HI, Februrary 2013, Paper number AAS 13-479.

[5] Ortega, P., Lopez-Rodriguez, G., Ricart, J., Dominguez, M., Castaner, L., Quero, J., Tarrida, C., Garcia, J., Reina, M., Gras, A., and Angulo, M., "A Miniaturized Two Axis Sun Sensor For Attitude Control of Nano-satellites," *IEEE Sensors Journal*, Vol. 10, No. 10, October 2010, pp. 1623 – 32, doi: 10.1109/JSEN.2010.2047104.

[6] Wu, S.-F. and Steyn, W. H., "Modelling and in-orbit calibration practice of a miniature 2-axis analogue Sun sensor," *Aerospace Science and Technology*, Vol. 6, No. 6, October 2002, pp. 423 – 33.

[7] Rufino, G., Grassi, M., and Rolfi, M., "Preliminary calibration results for a high-precision CMOS sun sensor," *Proceedings of the AIAA Guidance, Navigation, and Control Conference*, Honolulu, HI, August 2008.

[8] Bhanderi, D. D. V., *Spacecraft Attitude Determination with Earth Albedo Corrected Sun Sensor Measurements*, Ph.D. thesis, Aalborg University, Aalborg, Denmark, August 2005.

[9] Springmann, J. C., Sloboda, A. J., Klesh, A. T., Bennett, M. W., and Cutler, J. W., "The Attitude Determination System of the RAX Satellite," *Acta Astronautica*, Vol. 75, 2012, pp. 120–135, doi: 10.1016/j.actaastro.2012.02.001.

[10] Taraba, M., Rayburn, C., Tsuda, A., and MacGillivray, C., "Boeing's CubeSat TestBed 1 Attitude Determination Design and On-Orbit Experience," *Proceedings of the AIAA/USU Conference on Small Satellites*, Logan, UT, August 2009.

[11] Ovchinnikov, M., Ilyin, A., Kupriynova, N., Penkov, V., and Selivanov, A., "Attitude dynamics of the first Russian nanosatellite TNS-0," *Acta Astronautica*, Vol. 61, No. 1-6, 2007, pp. 277 – 285, DOI: 10.1016/j.actaastro.2007.01.006.

[12] Allgeier, S. E., Mahin, M., and Fitz-Coy, N. G., "Design and analysis of a coarse sun sensor for pico-satellites," *Proceedings of the AIAA Infotech at Aerospace Conference and Exhibit and AIAA Unmanned...Unlimited Conference*, AIAA, Seattle, WA, United states, April 2009.

[13] Springmann, J. C., Kempke, B. P., Cutler, J. W., and Bahcivan, H., "Initial Flight Results of the RAX-2 Satellite," *Proceedings of the 26th Annual AIAA/USU Conference on Small Satellites*, Logan, Utah, August 2012, Paper number SSC12-XI-5.

[14] Springmann, J. C. and Cutler, J. W., "Initial Attitude Analysis of the RAX Satellite," *Proceedings of the AIAA/AAS Astrodynamics Specialist Conference*, Girdwood, Alaska, 2011, Paper number AAS 11-600.

[15] Shuster, M. D., Pitone, D. S., and Bierman, G. J., "Batch Estimation of Spacecraft Sensor Alignments I. Relative Alignment Estimation," *Journal of the Astronautical Sciences*, Vol. 39, No. 4, October-December 1991, pp. 519–546.

[16] Shuster, M. D. and Pitone, D. S., "Batch Estimation of Spacecraft Sensor Alignments II. Absolute Alignment Estimation," *Journal of the Astronautical Sciences*, Vol. 39, No. 4, October-December 1991, pp. 547–471.

[17] Alonso, R. and Shuster, M. D., "Complete linear attitude-independent magnetometer calibration," *Journal of the Astronautical Sciences*, Vol. 50, No. 4, 2003, pp. 477 – 490.

[18] Foster, C. C. and Elkaim, G. H., "Extension of a two-step calibration methodology to include nonorthogonal sensor axes," *IEEE Transactions on Aerospace and Electronic Systems*, Vol. 44, No. 3, July 2008, pp. 1070 – 1078, doi: 10.1109/TAES.2008.4655364.

[19] Springmann, J. C. and Cutler, J. W., "Attitude-Independent Magnetometer Calibration with Time-Varying Bias," *Journal of Guidance, Control, and Dynamics*, Vol. 35, No. 4, June-July 2012, pp. 1080–1088, doi: 10.2514/1.56726.

[20] Pittelkau, M. E., "Kalman Filtering for Spacecraft System Alignment Calibration," *Journal of Guidance, Control, and Dynamics*, Vol. 24, No. 6, November-December 2001, pp. 1187–1195.

[21] Lai, K.-L., Crassidis, J., and Harman, R., "In-Space Spacecraft Alignment Calibration Using the Unscented Filter," *AIAA Guidance, Navigation, and Control Conference*, Austin, TX, August 2003, AIAA paper number 2003-5563.

[22] Duan, F., Liu, J., Li, R., and Li, D., "Real-time attitude-independent sun-sensor/magnetometer calibration algorithm for micro-satellite," *Proceedings of the SPIE - The International Society for Optical Engineering*, Vol. 5985, Wuhan, China, October 2005, pp. 598548–1–5.

[23] Reid, D., "Calibration of the Milstar attitude determination system," *Proceedings of the 1997 American Control Conference*, Albuquerque, NM, June 1997.

[24] Crassidis, J. L., Markley, F. L., and Cheng, Y., "Survey of Nonlinear Attitude Estimation Methods," *Journal of Guidance, Control, and Dynamics*, Vol. 30, No. 1, January-February 2007, pp. 12–28.

[25] Crassidis, J. L. and Markley, F. L., "Unscented filtering for spacecraft attitude estimation," *Journal of Guidance, Control, and Dynamics*, Vol. 26, No. 4, July-August 2003, pp. 536–542.

[26] Crassidis, J. L. and Junkins, J. L., *Optimal Estimation of Dynamic Systems*, Chapman and Hall/CRC, 2004.

[27] Lefferts, E., Markley, F., and Shuster, M., "Kalman Filtering for Spacecraft Attitude Estimation," *Journal of Guidance, Control, and Dynamics*, Vol. 5, No. 5, September-October 1982, pp. 417–429.

[28] Markley, F. L., "Attitude Error Representations for Kalman Filtering," *Journal of Guidance, Control, and Dynamics*, Vol. 26, No. 2, March-April 2003, pp. 311–317.

[29] Bhanderi, D. D. V., "Modeling earth albedo currents on sun sensors for improved vector observation," *Proceedings of the AIAA Guidance, Navigation, and Control Conference*, Keystone, CO, August 2006, Paper number AIAA 2006-6592.

[30] Bhanderi, D. D. V. and Bak, T., "Modeling earth albedo for satellites in earth orbit," *Proceedings of the AIAA Guidance, Navigation, and Control Conference*, San Francisco, CA, August 2005, Paper number AIAA 2005-6465.

[31] Cutler, J. W. and Bahcivan, H., "The Radio Aurora Explorer – A Mission Overview," *AIAA Journal of Spacecraft and Rockets*, 2013, In-print.

[32] Psiaki, M. L., Martel, F., and Pal, P., "Three-axis attitude determination via Kalman filtering of magnetometer data," *Journal of Guidance, Control, and Dynamics*, Vol. 13, No. 3, May-June 1990, pp. 506–514.

[33] Burton, R., Rock, S., Springmann, J., and Cutler, J., "Online Attitude Determination of a Passively Magnetically Stabilized Spacecraft," *Proceedings of the 23rd AAS/AIAA Spaceflight Mechanics Meeting*, Kauai, HI, Februrary 2013.

[34] Appel, P., "Attitude estimation from magnetometer and earth-albedo-corrected coarse sun sensor measurements," *Acta Astronautica*, Vol. 56, No. 1-2, January 2005, pp. 115–126, doi: 10.1016/j.actaastro.2004.09.001.